

RESEARCH ARTICLE

10.1002/2017GC006888

Key Points:

- Fractures in the Cretaceous–Paleogene of Jordan formed in response to volume loss during silica diagenesis
- Nevertheless, early fractures filled with carbonate cements as they formed
- Volume-reducing diagenetic reactions can therefore create fracture porosity, which can be filled by unrelated material

Correspondence to:

J. N. Hooker,
john.hooker@earth.ox.ac.uk

Citation:

Hooker, J. N., J. M. Huggett, J. Cartwright, and M. Ali Hussein (2017), Regional-scale development of opening-mode calcite veins due to silica diagenesis, *Geochem. Geophys. Geosyst.*, 18, 2580–2600, doi:10.1002/2017GC006888.

Received 24 FEB 2017

Accepted 5 JUN 2017

Accepted article online 15 JUN 2017

Published online 13 JUL 2017

Regional-scale development of opening-mode calcite veins due to silica diagenesis

John N. Hooker¹ , Jennifer M. Huggett², Joe Cartwright¹, and Mohammad Ali Hussein³ 
¹Department of Earth Sciences, University of Oxford, Oxford, UK, ²Department of Earth Sciences, Natural History Museum, London, UK, ³Geological Mapping Division, Ministry of Energy and Mineral Resources, Amman, Jordan

Abstract The formation and distribution of natural fractures in Cretaceous–Paleogene strata in Jordan are strongly tied to diagenetic processes, which in turn reflect the lithology of the host material. Observations collected from subsurface cores show that widespread fracturing began before compaction of the host sediment was complete, based on ptigmatic folding of one set of mineral-filled fractures (veins). Nonfolded veins are preferentially developed within heavily cemented layers. Calcium carbonate is the greatest volumetric component of the host sediment, and most fractures are at least partially filled by calcite. Dolomite-bearing and silica-bearing fractures are present in dolomitized and silicified host beds, respectively. Horizontal veins are filled by cone-in-cone calcite or, rarely, silica or dolomite. The stratigraphic arrangement and degree of compaction around ptigmatically folded calcite veins and chert nodules suggest that silica diagenesis was an important driver of early fractures. Nevertheless, those fractures were filled with carbonate cements as they opened, based on crack-seal texture of the vein fill. The volume loss associated with silica diagenesis created fracture porosity, which was filled coevally by carbonate cements. The distribution of later veins reflects embrittlement of host layers by cementation and is consistent with crustal deformation as the primary fracture driver.

Plain Language Summary This paper describes natural fractures in mudrocks from Jordan. We present various lines of evidence that the fractures formed in response to volume loss associated with the transformation of opal into quartz (i.e., silica diagenesis) during early burial. Interestingly, these fractures also filled with calcite while they opened. Calcite is not directly involved in silica diagenesis. Therefore, this paper presents new evidence that chemical reactions can open fracture pore space in rocks, and that that space can be filled by another material. This sequence implies that the permeability of the host material can be affected by the development of chemically induced fractures.

1. Introduction

Fractures in stratified rocks are commonly preferentially developed within certain layers or groups of layers. Which layers become fractured will depend on the nature of the driving stresses as well as the mechanical properties of the beds and their interfaces during fracturing. For example, if fractures are driven by extension that is homogeneous across strata, then preferential fracturing may be expected in the stiffest layers [e.g., Ferrill *et al.*, 2014], all else being equal. Alternatively, if applied stress is a constant boundary condition, then the strain energy available to create fractures may be higher in less stiff layers [Price, 1966]. If fracture propagation is maintained by injection of fluids into the fractures amid remote compression, then stiffer layers will be more effective at arresting fracture propagation [Gudmundsson and Brenner, 2001]. Tensile fractures can initiate amid remote compression where layers of contrasting mechanical properties are bonded to one another [Bourne, 2003]. Weak bedding interfaces can also arrest fracture propagation by enabling sliding between layers [Cooke and Underwood, 2001].

Furthermore, diagenetic reactions and other processes can cause rock mechanical properties to change over time, such that those layers currently most susceptible to fracture may not have always been so [Shackleton *et al.*, 2005; Ortega *et al.*, 2010; Lavenue *et al.*, 2013; Giorgioni *et al.*, 2016]. The variety of observed fracture-stratigraphic patterns motivated the concept of *fracture stratigraphy* [Laubach *et al.*, 2009], being a descriptive approach to the problem, in contrast to the approach of *mechanical stratigraphy*, which emphasizes the mechanical properties of layers for fracture prediction.

Preferential fracturing of layers may also be unrelated to mechanical properties per se; for example, fractures may be generated in mudrocks by in situ hydrocarbon maturation [Jochum *et al.*, 1995; Zhang *et al.*, 2016], and thus be absent from neighboring layers having lower organic content and higher permeability. As well, fracturing can be driven by volume-changing diagenetic reactions within the host [Shearman *et al.*, 1972; Ulven *et al.*, 2014].

In the present study, we focus on an organic-rich mudrock succession from Jordan that bears a highly stratified regional fracture pattern. Fracture orientation, fill, morphology, and stratigraphic distribution all point to interrelated host lithology, diagenesis, and fracturing. The sequence is fine-grained throughout, and therefore has little obvious mechanical stratification except that provided by diagenetic processes, particularly silica diagenesis. The present study highlights the capability of diagenesis (i) to impact fracture distribution, by creating mechanical contrasts to rock layers via cementation of pore space, and (ii) to generate fractures via mineralogic volume changes. With respect to the latter, this study documents fracture opening and sealing by calcite coincident with silica diagenesis, thus demonstrating that vein fill mineralogy does not necessarily reflect the diagenetic process responsible for opening fractures.

The capability for diagenetic reactions to create opening-mode fractures has important implications for interpretations of tectonic events and styles, primarily in the sense that diagenetic deformation should not be mistaken for tectonic deformation. Moreover, in connection with hydrocarbon exploration or CO₂ sequestration, it should be considered that, in addition to the potential for diagenetic processes to occlude or create pore space by precipitation or dissolution, respectively, such processes may actually impart stresses to the rock and lead to fracturing. In general, our understanding of the dynamics between subsurface deformation, fluid flow, and diagenesis is yet in its infancy.

2. Geologic Setting

The Muwaqqar Formation was deposited in the northward-prograding Sirhan Basin (Figure 1) along the southern margin of the Tethys Ocean [Powell and Moh'd, 2011]. The mudrock is high in organic carbon, locally in excess of 20 wt % [Ali Hussein *et al.*, 2014], and is known informally as the Jordan Oil Shale. Accommodation for the sediment was mostly provided by extension along NW-SE striking normal faults [Abu-Jaber *et al.*, 1989; Lüning and Kuss, 2014]. Active faulting during sedimentation resulted in restriction of subbasins and sediment reworking [Alqudah *et al.*, 2014]. Low organic maturity suggests a maximum burial depth

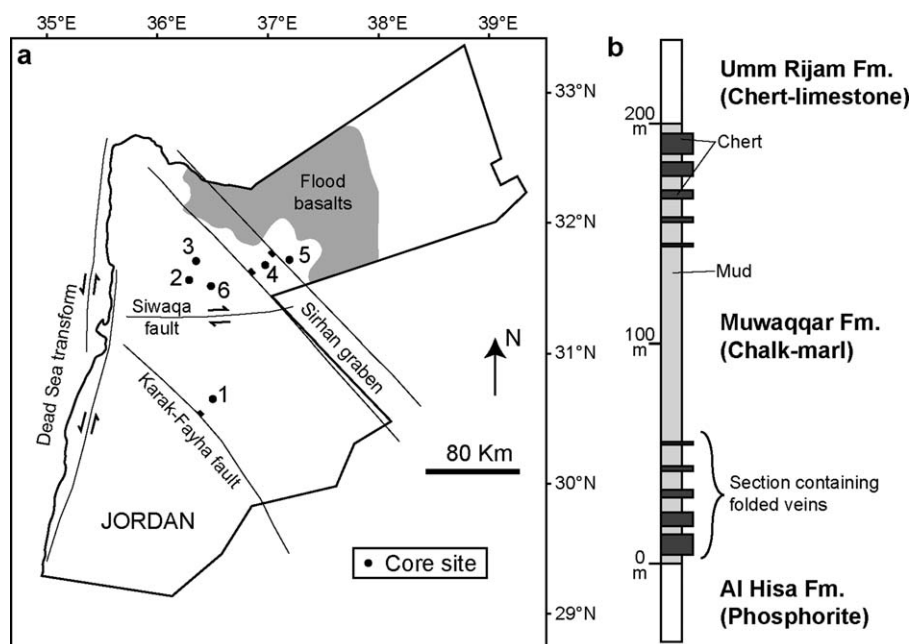


Figure 1. (a) Geographic location of studied cores. (b) Stratigraphy, based on Belqa Group [Powell and Moh'd, 2011], with schematic distribution of chert.

near 1.5 km for the Muwaqqar Formation in general. Alpine shortening produced regional exhumation [Abu-Jaber *et al.*, 1989], placing most current sample depths between 300 and 600 m.

The cored host-rocks comprise variable proportions of calcite, quartz, organic matter, and apatite, with locally abundant chalcedony, dolomite, minor pyrite, and sphalerite, plus smectite and trace illite in marl layers. In the study area, clay is typically a very minor component, despite the formation's classic designation as a chalk-marl [Powell and Moh'd, 2011, and references therein]. Quartz is generally microcrystalline; local radiolaria fossils are present. Carbonate and chert nodules are abundant. Chert beds and nodules are developed along individual beds near the top and bottom of the Muwaqqar Formation (Figure 1).

3. Methods

Fractures were logged in core using a 10X hand lens. Fractures were identified as natural based on the presence of mineral cements or bitumen infill. Completely barren fractures were locally observed but ignored in this study because such fractures may have formed during core drilling or handling. Carbonate minerals were distinguished at the core scale using scratch tests and HCl. No information on core declination is available; we assume that the core is vertical, based on bedding generally lying at right angles to the core.

Scanning electron microscope (SEM) analyses were performed on an FEI Quanta 650 field-emission gun with cathodoluminescence (CL) and energy-dispersive X-ray spectroscopy (EDS) detectors. All SEM operations were performed at 20 kV and 10 mm working distance.

4. Fracture Description and Distribution

4.1. General Observations

Natural fractures are present throughout all cores observed. Fractures were systematically logged in Cores 1–5 (Table 1). Below we describe the stratigraphic distribution of fractures in Cores 2 and 3 (Figure 2), which sample three stratigraphic Units (A–C) defined by the presence (A and C) versus absence (B) of chert in the section [Ali Hussein *et al.*, 2014]. All three units are rich in organic matter, containing commonly 10 wt %, and locally exceeding 20 wt %, organic carbon.

Units A and C contain abundant nodular and bedded chert. In many cases, sedimentary laminae wrap around cherts, indicating a nodular geometry to the chert. In other cases, chert boundaries are horizontal as are laminae within and outside cherts, suggesting a tabular geometry, at least where the core intersects the chert. Most layers within Unit B contain 5–20 wt % nondetrital silica, interpreted as biogenic in origin [Huggett *et al.*, 2017], but the unit lacks macroscopic chert entirely.

The cores contain opening-mode fractures and faults. Opening-mode fractures generally have steep dips, near orthogonal to horizontal beds, and have sub-mm-scale to mm-scale opening displacements (Table 1) and cm-scale to dm-scale heights. Exceptions include horizontal fractures and rare obliquely dipping fractures, which may be orthogonal to rare slumped beds. Most opening-mode fractures are present in bed-bound arrays, with fracture spacing closer in thinner layers. Where multiple fractures are present in a given layer, fractures may strike parallel to one another or show little or no preferred orientation. There is a greater tendency for strike-dispersion within folded veins and veins in nodular-cemented layers, compared to the relatively parallel arrays of planar veins outside nodules. The true strike of fractures is unconstrained in this paper because the core is not oriented.

Table 1. Summary of Logged Fracture Aperture Data, Cores 1– and 5^a

	Planar and Vertical					Layer-Parallel		
	Folded Calcite Veins	Nonnodular	Carbonate Nodules	Silica Nodules, Silica Fill	Silica Nodules, Carbonate Fill	Silica	Dolomite	Bitumen
N	899	787	52	215	665	57	3	23
Average	0.35	0.48	0.40	0.32	0.36	0.42	0.76	0.37
stdev	0.27	0.55	0.42	0.30	0.59	0.27	0.35	0.31
Max	2.15	5	2.65	2.65	12	1.4	1.15	1.15
Median	0.265	0.33	0.265	0.265	0.215	0.33	0.62	0.265

^aVeins counted as bitumen are filled primarily with bitumen and contain little or no mineral cement.

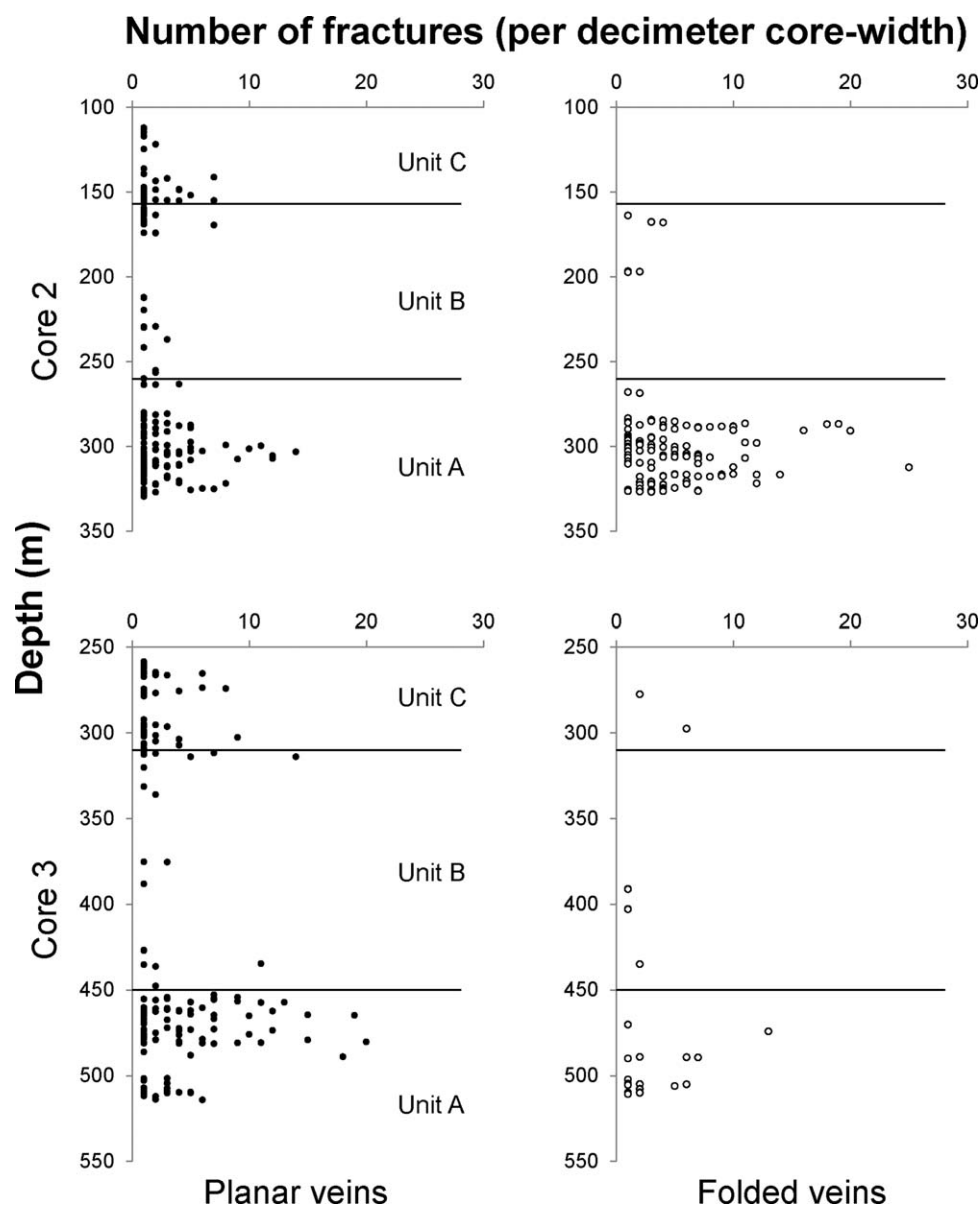


Figure 2. Stratigraphic distribution of folded and planar veins, Cores 2 and 3.

Fractured layers are dominantly carbonate and silicate cemented; marl layers are less commonly and less intensely fractured. Within nodules, fractures tend to link and splay, in extreme cases forming brecciated fabrics.

Most opening-mode fractures have planar walls, but a substantial fraction (Table 1) is ptlygmatically folded. We describe the folding in detail and interpret its cause below. Folded veins are most common in Unit A (Figure 2); planar veins are common in Units A and C.

4.2. Fracture-Stratigraphic Distribution

Most opening-mode fractures appear bound within their host beds; i.e., their tips coincide with bedding boundaries. Silica-filled and dolomite-filled fractures are almost exclusively found in silicified and dolomitized layers, respectively. Calcite-filled fractures are present in all types of layers.

The majority of fractures in Unit A are cemented by low Mg calcite, either solely or as a late phase in fractures and faults with early dolomite, silica, and kaolinite. Rare barite occurs in the center of calcite-

cemented fractures. Macroscopic bitumen is rare in Unit A fractures, but micron-scale bitumen inclusions are present within both carbonate and quartz cements.

Fractures are relatively rare in Unit B (Figure 2). Fractures are generally planar and sealed with calcite, commonly tall (dm-scale or taller), and widely spaced, such that generally only one or two fractures are preserved at any core depth. Cone-in-cone calcite has crosscut dolomite-cemented marl and includes seams of dolomite and organic matter.

Fractures are widely developed in Unit C and are cemented by calcite. Bitumen is common in these fractures, particularly in shear fractures. At the core scale, bitumen may entirely fill fractures or be present amid visible cement deposits. Microscopic inclusions of bitumen are present within cements, as described below. Faults are by far the most common in Unit C compared to A and B.

4.3. Faults

Shear-mode fractures (faults) commonly dip 50° – 80° , with normal offset (Figures 3a–3c). Displacement can be mm scale or greater; large displacements are difficult to quantify owing to the short core-fault intersection. Faults can be discrete or have broad damage zones of up to dm-scale thickness; damage zones can include brittle cracking and plastic deformation.

Calcite is the most common fault cement. As with opening-mode fractures, dolomite and silica cements are common in faults within dolomitic and silicic beds, respectively (Figure 3d).

4.4. Planar Veins

Planar calcite veins are most commonly hosted within marl layers of Unit B and silicified layers in Units A and C. Within Unit B, calcite vein walls are commonly rugose on a submillimetric scale, producing a crenulated appearance at the fracture wall. This irregularity is usually inconspicuous given the mm-scale to cm-scale aperture and up to m-scale length (height) of these veins (Figure 4b). Apertures decrease systematically toward upper and lower tips from maximum values that are close to uniform along fracture lengths. Marl-hosted planar calcite veins are close to orthogonal to bedding, but deviate up to 20° from this geometry. Where more than one fracture in a layer is present in the core, multiple fractures may be parallel or deviate in strike up to roughly 30° , suggesting that planar calcite veins are present in roughly parallel sets. In addition, visible fractures are often composed of microscopic bands of cement extending parallel to the fracture and commonly including solid bitumen or organic-rich host-rock amid the cement (Figure 4c). These are interpreted as crack-seal bands [Ramsay, 1980], and also compose parallel microscopic fractures (Figure 4d). This pattern is consistent with pervasive microfractures parallel to macroscopic fractures in tight gas sandstones and their analogues [Hooker *et al.*, 2014].

Chert-hosted calcite veins are exclusively planar; some chert-hosted veins extend outside cherts into the marls where they are folded; such veins are described in the next section. Like marl-hosted veins, calcite veins within chert may dip as much as 20° from vertical and generally cut across their host nodule or layer entirely. Relative to marl-hosted veins, chert-hosted veins are closely spaced, have greater strike variation, and show a greater tendency to link with nearby veins, such that chert layers may appear brecciated by calcite veins.

Silica veins are found almost exclusively in silicified layers or nodules. Such veins are lined, and generally sealed, with silica cement, although many also contain calcite cement. Silica veins are mostly planar, with sharp boundaries (Figure 5b). There may be multiple orientations present within individual nodules.

Within silica veins, calcite commonly fills the center of veins, with rinds of silica cement lining the vein walls (Figure 5c). Crosscutting relationships between such bimineralic veins suggest repeated phases of silica and carbonate cementation (Figure 5c).

Dolomite-bearing veins are rare compared to calcite and silica veins. Some silica-bearing veins are dominantly dolomite-filled where the vein cuts heavily dolomitized strata. Cathodoluminescence and EDS maps indicate fracture-filling dolomite overgrows host-rock dolomite, and that the host-rock dolomitization preceded fracture filling (Figure 5b). Dolomite rhombs typically include bitumen and are present amid bitumen fill and late calcite. Fracture-filling dolomite overgrows host-rock dolomite rhombs and interfingers with fracture-filling silica.

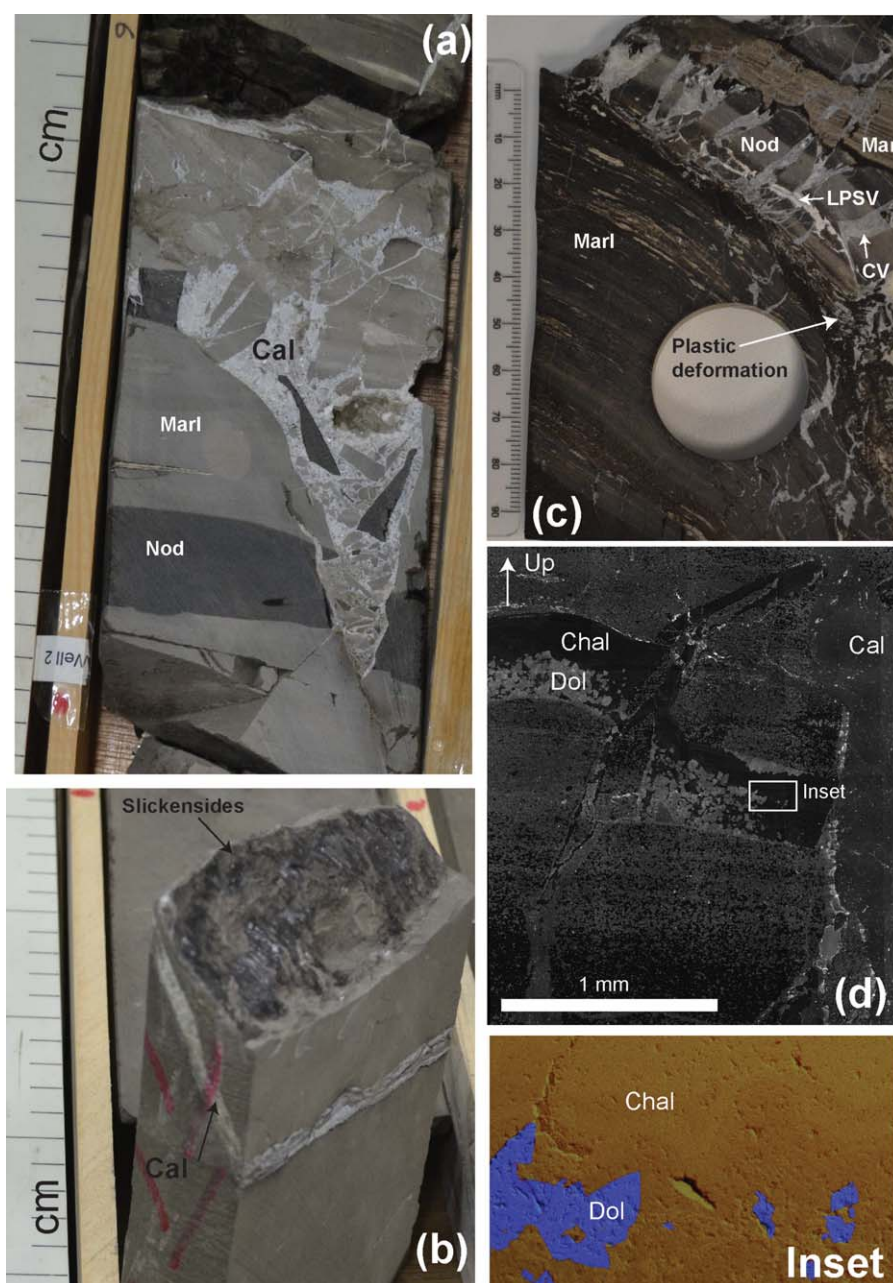


Figure 3. Faults. Nod, nodule; LPSV, layer-parallel silica vein; CV, calcite vein; Cal, calcite; Chal, chalcedony; Si, silica; Dol, dolomite. (a) Core 3, Unit C. Calcite-cemented fault zone brecciates a chert layer and surrounding mudrock. (b) Core 3, Unit B. Relatively discrete fault dips approximately 70°. Fault is calcite-cemented with dip-slip slickensides in carbonaceous matter. (c) Core 6. Distributed deformation in a fault zone. Note how deformation in dolomite and silica nodules is brittle and that in adjacent marls is plastic. Also note changes in thickness of laminated marl overlying nodule, possibly as a result of mobilization of the intervening, organic-rich (dark) layer. (d) Fault zone cutting chalcadony-dolomite layer, Core 6. In the host-rock, dolomite and silica follow sedimentary gradations. Within the fault, dolomite rhombs have formed around cataclastic material that collected at the bottom of the fault; this dolomite is overgrown by botryoidal chalcedony. Calcite cement crosscuts chalcedony and dolomite. (inset) EDS-SEM map false-colored for calcium and silicon.

4.5. Folded Veins

Folded veins are present almost exclusively in Unit A. Such veins are dominantly calcite filled but locally contain microcrystalline silica and trace minerals such as barite. Folded veins are generally hosted in marl layers close to chert layers, which may host planar veins (Figures 6a–6c). Some of the folded veins are planar where they cut silicified layers and then only become tightly folded where they cut the intervening unsilicified marls (Figure 6a). Folded veins may be isolated or present in layer-bound arrays. Sedimentary laminae

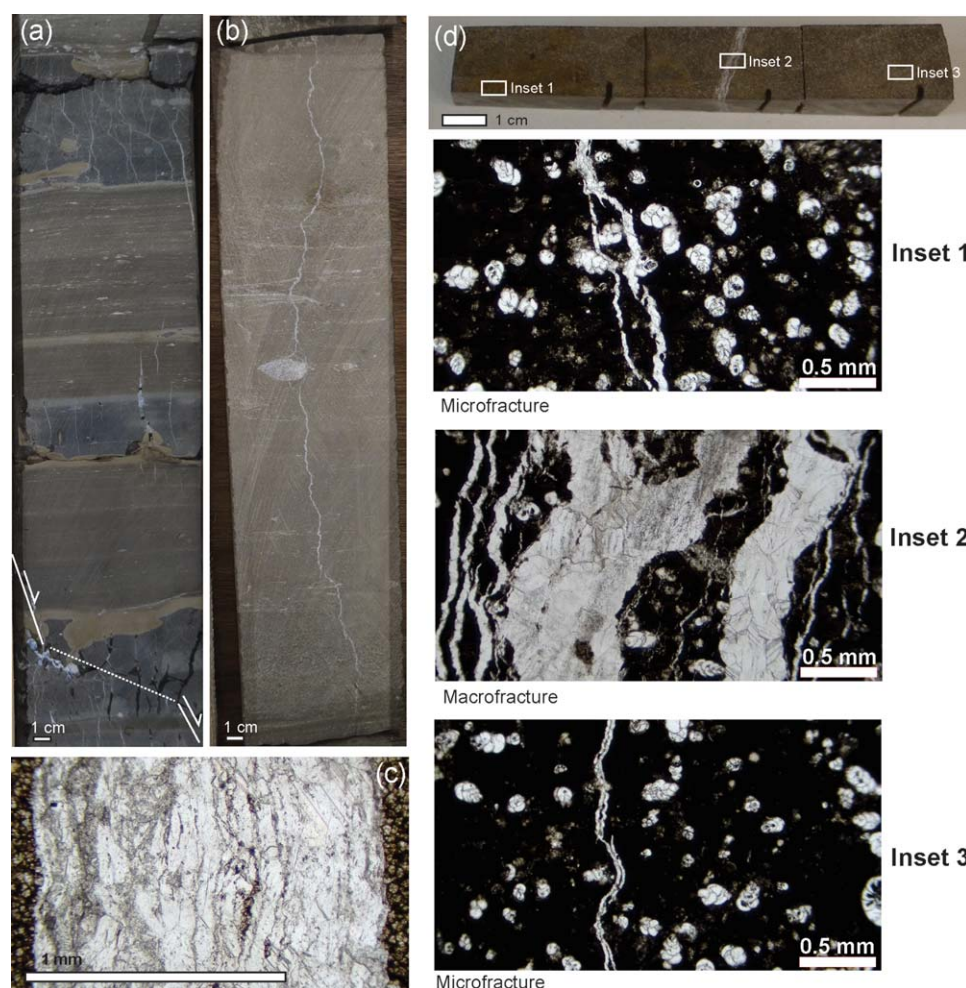


Figure 4. Planar calcite veins. (a) Core 3, Unit A. Note veins preferentially cut chert layers, and low-offset fault cutting chert layer at bottom. (b) Core 3, Unit B. Calcite vein bound to thick marl bed. Rugosity of fracture plane is exaggerated owing to low angle between fracture plane and core face. (c) Plane-polarized light image of fracture in Figure 4b. Note crack-seal increments separated by host-rock slivers, implying incremental opening and sealing. (d) Macroscopic calcite vein (“macrofracture”) with parallel and subparallel “microfractures” (insets 1–3), Core 2 Unit B.

may be variably compacted near the tips of folded veins (Figure 6a). Folded veins are absent from coarse-grained layers such as reworked conglomerates and skeletal limestones.

The folding is interpreted to be caused by vertical compaction (see below) and produces near-sinusoidal traces on core faces (Figures 6a–6c). These structures are interpreted as veins on the basis of the straightness of their traces on bedding planes, planarity within competent chert beds, crack-seal texture within cement, crosscutting of host-rock grains, and branching geometry.

Folded calcite veins are typically much shorter than their planar counterparts, with present-day heights generally less than 5 cm. We discuss their original (straight-line) heights in the compaction section below; most original heights are on the order of twice the present-day height, such that their original height was still much shorter than that of most currently planar veins.

Cement within folded veins may be coarsely blocky or have micron-scale crack-seal bands, marked by single-phase fluid inclusions (Figures 7a and 7c). Calcite cement contains abundant twin planes (Figures 7b and 7c). Twin thickness and intensity typically do not increase within fold hinges. Twins are commonly bent with folds within fold hinges. Stylolites are more common in fold hinges than in limbs (Figure 7c).

In a rare example in which biosiliceous microfossils are preserved (Figure 8), a calcite vein is folded within a bed containing calcite-replaced radiolaria and planar within a bed containing chert-cemented radiolaria.

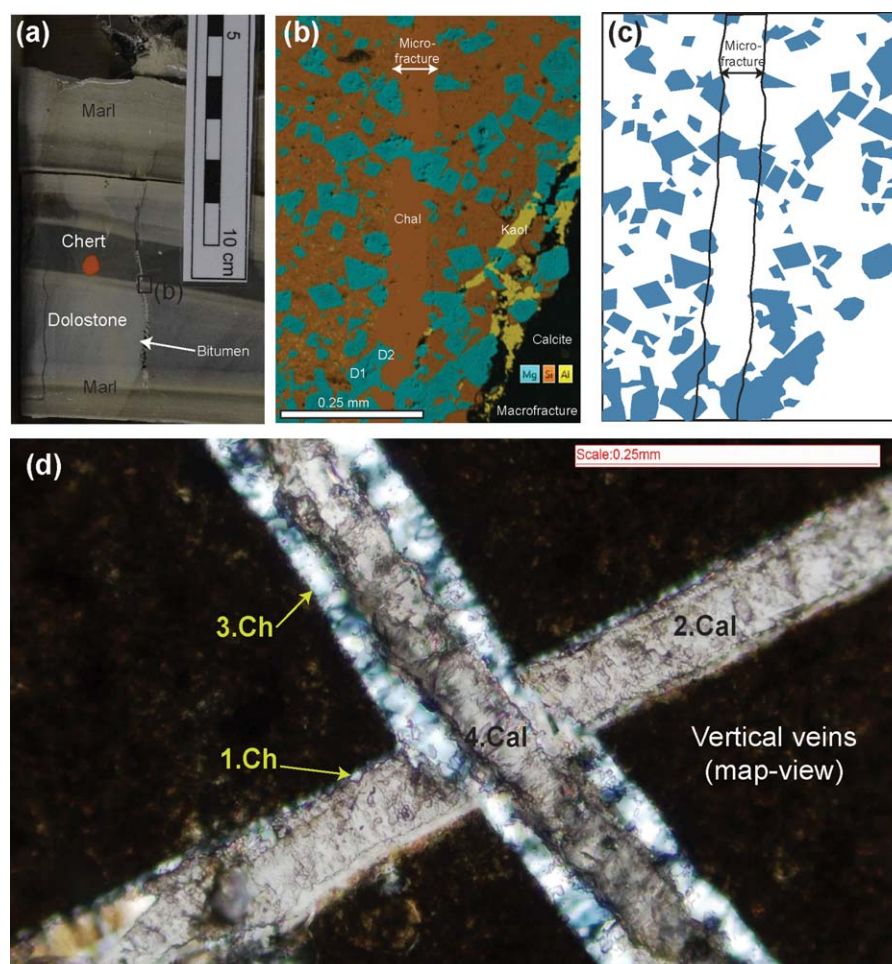


Figure 5. Vertical, chalcedony-filled and carbonate-filled fractures. Cal, calcite; Chal, chalcedony; D1, early dolomite; D2, late dolomite; Kaol, kaolinite. (a) Core 5, vertical fracture cuts dolomitized and silicified layers. (b) EDS map of fracture in Figure 5a. The macrofracture is mostly filled with calcite and bitumen but lined with early kaolinite. A nearby microfracture in Figure 5b is filled mostly with chalcedony but dolomite (D2) overlaps host-rock dolomite (D1) and interfingers with chalcedony cement, suggesting coprecipitation of the two fracture-cement phases. (c) Interpretation of Figure 5b, showing location of microfracture, and dolomite for reference. (d) Crosscutting vertical fractures in silicified interval, Core 2 Unit A. Crosscutting veins are lined with chalcedony and filled with calcite, likely indicating chalcedony predates calcite precipitation within each fracture, assuming syntaxial fill. But regardless of the relative cement timing within each vein, the chalcedony in the later vein appears to cut calcite in the earlier vein, suggesting alternating chalcedony and calcite precipitation.

Radiolaria are deposited as opal A. The chert in the sample takes the form of both chalcedony and microcrystalline quartz. Opal A transforms to denser, less soluble opal CT, chalcedony, or quartz via dissolution-reprecipitation at ambient or elevated temperatures [Williams and Crerar, 1985]. The radiolaria are generally uncompacted (Figures 8c and 8d). Therefore, whereas the calcified radiolaria represent locations of “missing” silica because they were originally opal A, the chertified radiolaria imply the presence of “excess” silica, which enabled the transformation of opal A to denser chert without volume loss. A simple interpretation is that within these beds, the opal A-chert transition involved bed-scale transfer of silica, from the now-calcified radiolaria to the now-chertified radiolaria. The source of the calcite is unclear, but it is in optical continuity with fracture-filling calcite, and the two are chemically indistinguishable using SEM-EDS.

4.6. Horizontal Veins

Horizontal veins are less common than vertical veins; most horizontal veins were encountered in Core 5. Crosscutting relationships between horizontal and vertical veins are rare and nonsystematic in their relative timing. In contrast to the polymineralic fill of many vertical veins, we have encountered layer-parallel calcite, dolomite, and silica veins having a dominant filling mineral with only trace (<1%) accessory minerals (Figures 9c and 9d). Horizontal dolomite veins may contain bitumen or pore space. Dolomite typically has

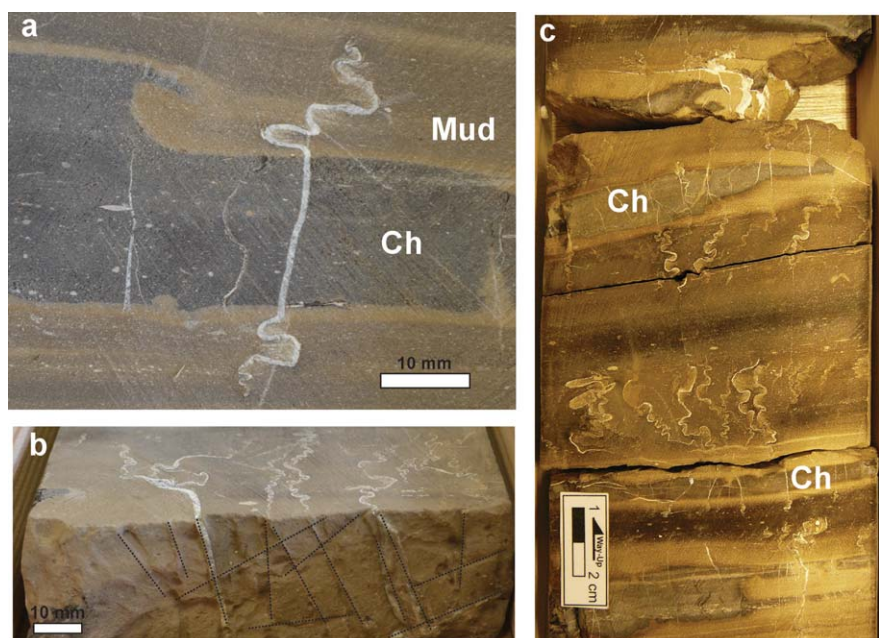


Figure 6. Folded calcite veins, Unit A, Core 2. (a) Calcite vein crosscutting chert (Ch) layer. Vein is planar within chert and folded within the matrix mud. (b) Folded veins in bed-parallel view. Traces (dashed) are straight and poorly aligned. (c) Folded and straight veins. Folded veins occur above and below chert nodules/layers.

euohedral faces, with bitumen and single-phase aqueous inclusions aligned parallel to those faces (Figure 9c). Chalcedony has a botryoidal form (Figure 9b).

Near the centers of fractures, microquartz overlaps chalcedony (Figures 9a and 9b). Microquartz-filled veins commonly crosscut chalcedony-filled veins; we never observed the opposite relationship. We interpret that the morphology of the chalcedony and microquartz fibers is consistent with void-filling precipitation; we find no evidence of precursor opaline cements within veins.

To the extent that cone-in-cone represents a displacive cement that forms layer-parallel sheets, it may be regarded as a monomineralic layer-parallel vein. Cone-in-cone is present in siliceous mud intervals (Figure 10). Cores 2 and 3 have conic calcite in Unit B and no other intervals, suggesting that the cone-in-cone is stratigraphically correlable. SEM images (Figures 10b and 10c) show that cone-in-cone structure is composed of calcite arrayed in conical masses separated by host-rock material. Calcite also fills radiolaria tests ensconced within the cones. Cone-in-cone appears to expand the sedimentary framework grains [Hooker and Cartwright, 2016], and thus displace the host-rock in a primarily vertical sense. Locally the displacive calcite forms strands oblique to bedding (Figures 10a and 10c). Cone-in-cone locally includes overgrowths of dolomite rhombohedra, suggesting host-rock dolomite formed before the cone-in-cone [Hooker and Cartwright, 2016].

5. Compaction Analysis

The finely laminated nature of many nodule-hosting beds in the core affords us a rare opportunity to quantify the degree of compaction that has occurred around nodules. We note thinning of laminae lateral to nodules, relative to their thickness within the nodule (Figure 11a). This thinning is accommodated by lateral thickening of laminae that overlie and underlie the nodule. For nodules that replace host material, including interstitial fluids, we can treat the height of laminae within the nodule as the original stratigraphic thickness of the section at the time the nodule formed. Where preserved in core, we can measure the same stratigraphic thickness lateral to the nodule, yielding a corresponding final thickness. The ratio of the two thicknesses is a measure of the amount of compaction that has occurred since the nodule formed. Thus, we define and can calculate a nodular compaction ratio (C_N) as

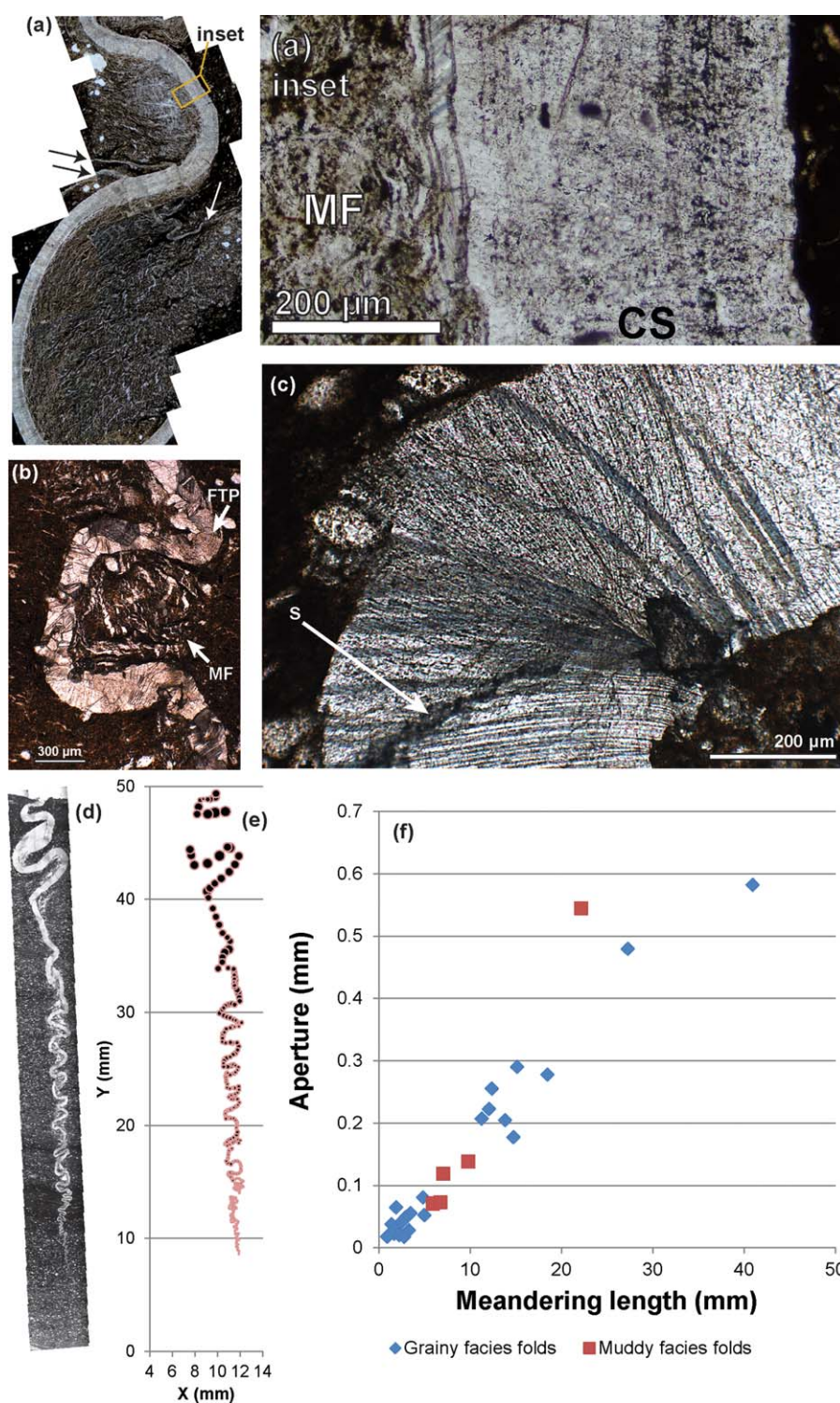


Figure 7. Petrography of folded calcite veins. FTP: folded twin planes; MF: microfractures; S: stylolite. (a) Core 2, Unit A. Note microfractures clustered within inner arcs of folded veins. (inset) Crack-seal texture signifying simultaneous opening and sealing with calcite. Crack-seal increments appear variably bent, with some forming highly arguate shapes within the microfractured inner arcs (arrowed in Figure 7a). (b) Core 5. Example with blocky calcite, folded twin planes, and microfractures clustered within inner arcs. (c) Core 5. Folded twin planes and stylolites near hinge of folded calcite vein. (d) Core 5. Plane-polarized light mosaic of folded calcite vein. Fracture cuts beds with ~50% radiolaria tests and intervening muddy (dark) beds. (e) Map of vein in Figure 7d with bubble area scaled to aperture. (f) Linear relationship between length of folds and aperture within fracture in Figure 7d, consistent with buckle folding of the calcite vein during host-rock compaction.

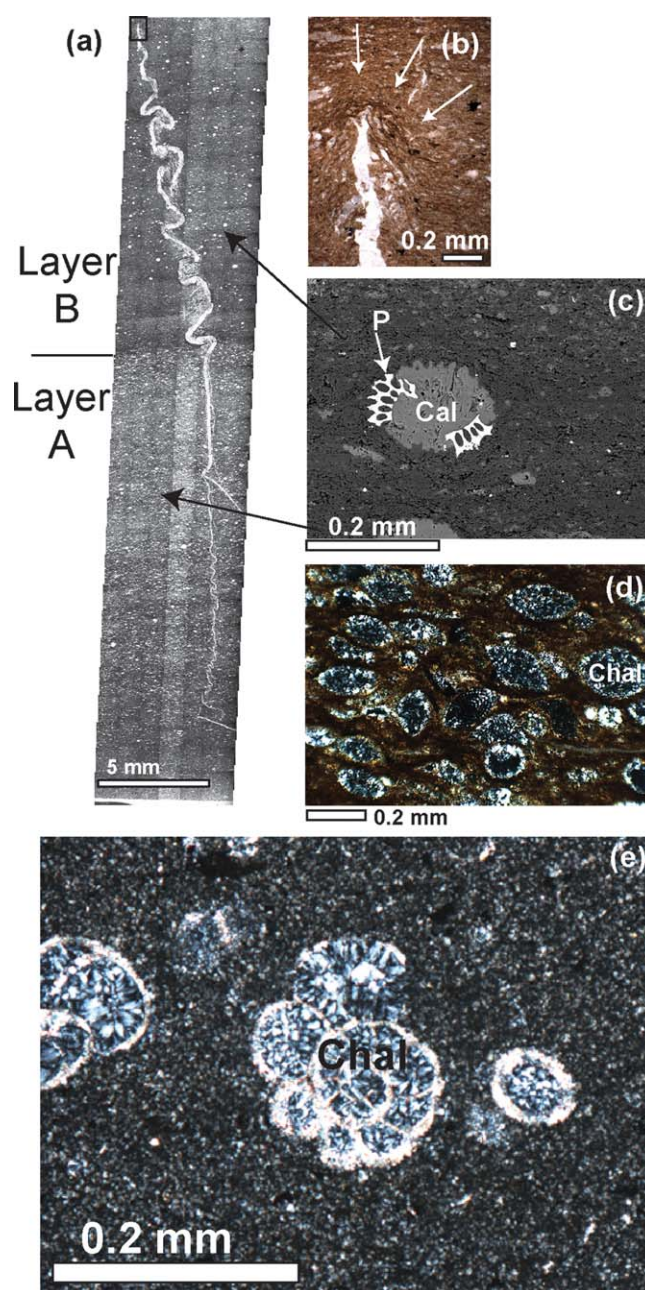


Figure 8. Partially folded calcite vein, Core 5. Cal, calcite; Chal, chalcedony; P, Pyrite. (a) Calcite vein that is planar in chert layer (Layer A) and folded in mud layer (Layer B). (b) Upper tip of calcite vein; note sedimentary laminae (arrowed) wrapping around the top. (c) Calcified and pyritized radiolaria test, illustrating originally silicate material now dissolved and replaced/filled by calcite in Layer B. (d) Chertified radiolaria test, illustrating original opal A now formed of chert without volume loss, implying addition of silica. (e) Foraminifera test now replaced and filled by chalcedony (silica).

compaction ratios for the silica nodules are significantly lower (1.3–4.6) than for the carbonate nodules. The compaction ratios for the folded veins are interesting in that they tightly cluster with a range of 1.7–2.2 (Figure 13).

6. Discussion

6.1. Stratigraphic Fracture Distribution

In all cores, we observe fractured and nonfractured layers. Some apparently unfractured layers likely have a wider fracture spacing, and so only appear to be unfractured in core. This sampling effect may be

$$C_N = \frac{T_N}{T_L} \quad (1)$$

where T_N is the (original) thickness of a stratigraphic package across the nodule vertically and T_L is the (compacted) thickness of the same package lateral to the nodule.

This method is inapplicable to nodules that displace the host material. Evidence that cements replaced host material or passively filled pore space, and thus are appropriate for compaction measurements, includes preserved internal lamination and cement in pore spaces among a self-supporting sedimentary framework [e.g., Sellés-Martínez, 1996]. In general, the silica and carbonate nodules appear to comprise pore-filling and sediment-replacing cements (Figures 8e and 11) as opposed to displacive cements such as cone-in-cone (Figure 10).

For folded calcite veins, we calculate a compaction ratio for veins as the meandering length of the vein (original length) divided by the present-day vertical distance between the vein tips (final length) [Hiscott, 1979] (Figure 12). We calculate the compaction ratio for veins (C_V) as

$$C_V = \frac{L_0}{L_1} \quad (2)$$

where L_0 is the meandering length of the vein (original length) and L_1 is the present-day vertical distance between the vein tips (final length). The meandering length will be exaggerated where the vein intersects the core face obliquely and so is corrected trigonometrically. We believe this measure of compaction to be a minimum estimate, for reasons discussed below.

Compaction ratios are highest around the carbonate nodules but there is a large range in the values from an upper limit of 6.7 to a lower value of 1.7. Com-

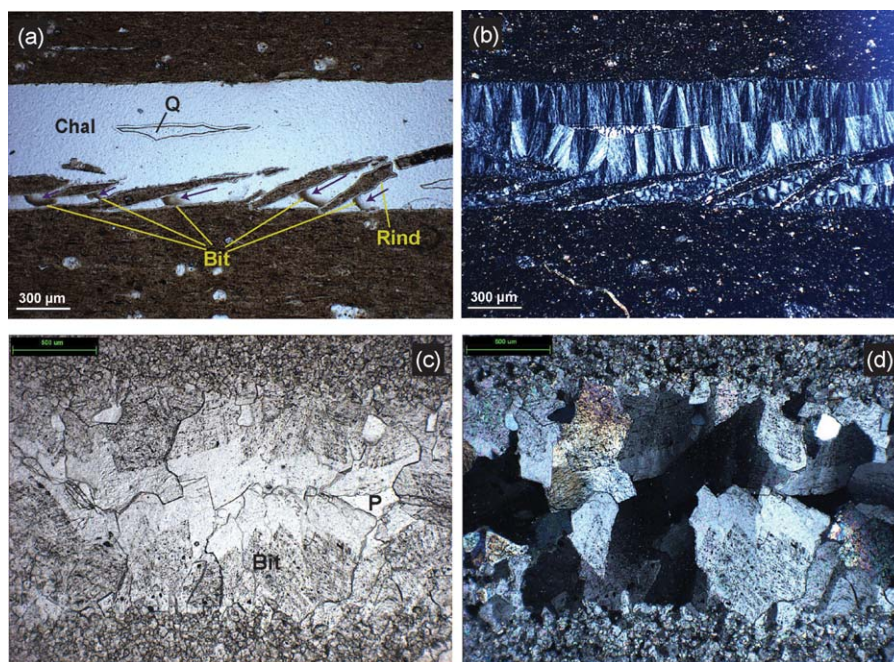


Figure 9. Horizontal veins in thin section, Core 5. Bit, bitumen; Chal, chalcedony; P, porosity; Q, quartz. (a) Silica vein, plane-polarized light. Note thin isopachous rind of silica lines the fracture walls. This rind is overlain by fan-shaped, botryoidal chalcedony, which in turn is overlain by microquartz. The botryoidal texture suggests precipitation along fracture walls into a fluid-filled void space, and thus the overlapping phases postdate those they overlap. Bitumen inclusions within chalcedony suggest bitumen was present during sealing, and suggest a migration direction for bitumen (from the diffuse side toward the discrete side, shown by arrows). (b) Same as Figure 9a in cross-polarized light. (c) Layer-parallel dolomite vein, plane-polarized light. Note euhedral faces with bitumen inclusions. (d) Same as Figure 9c in cross-polarized light.

particularly important within Unit B, because the fractures that were sampled by the core within that Unit are relatively tall, and the beds thick. Part of the reason for the thicker fractured beds is the absence of silicified horizons in Unit B, which tend to localize fractures in Units A and C.

In Unit C, the highest cumulative fracture aperture is manifest in planar calcite veins within the silicified layers. The reasons for preferential silicification were discussed by *Huggett et al.* [2017]; regardless, the consistent and near-perfect bedding-boundedness [*Hooker et al.*, 2013] of calcite veins within chert layers in

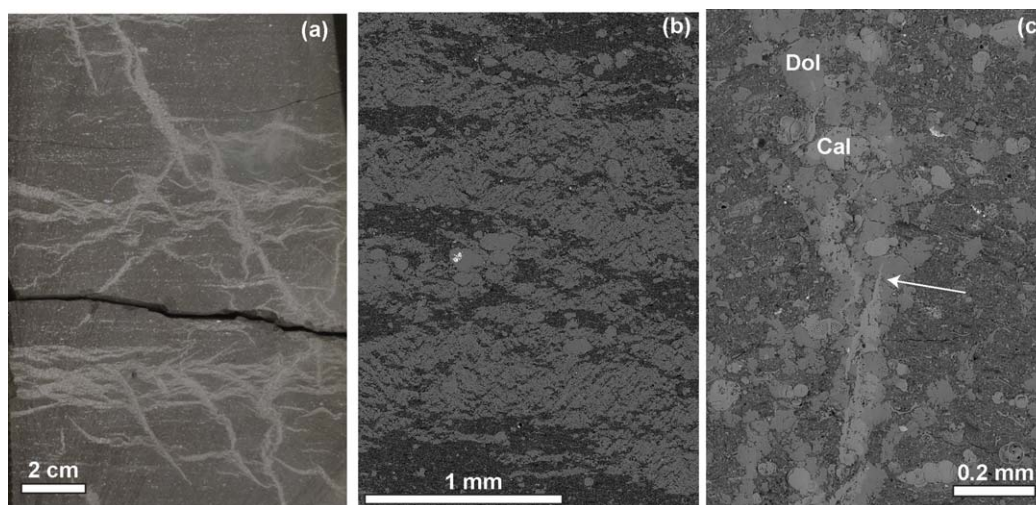


Figure 10. Cone-in-cone, Core 3, Unit B. Cal: calcite; Dol: dolomite. (a) In core, cone-in-cone appears as wispy, discontinuous layers of carbonate cement, generally extending parallel to bedding but locally crosscutting beds. (b) Backscattered electron (BSE) image of layer-parallel cone-in-cone segments. (c) BSE image of near-vertical cement strand within cone-in-cone structure. Note calcite cuts dolomite.

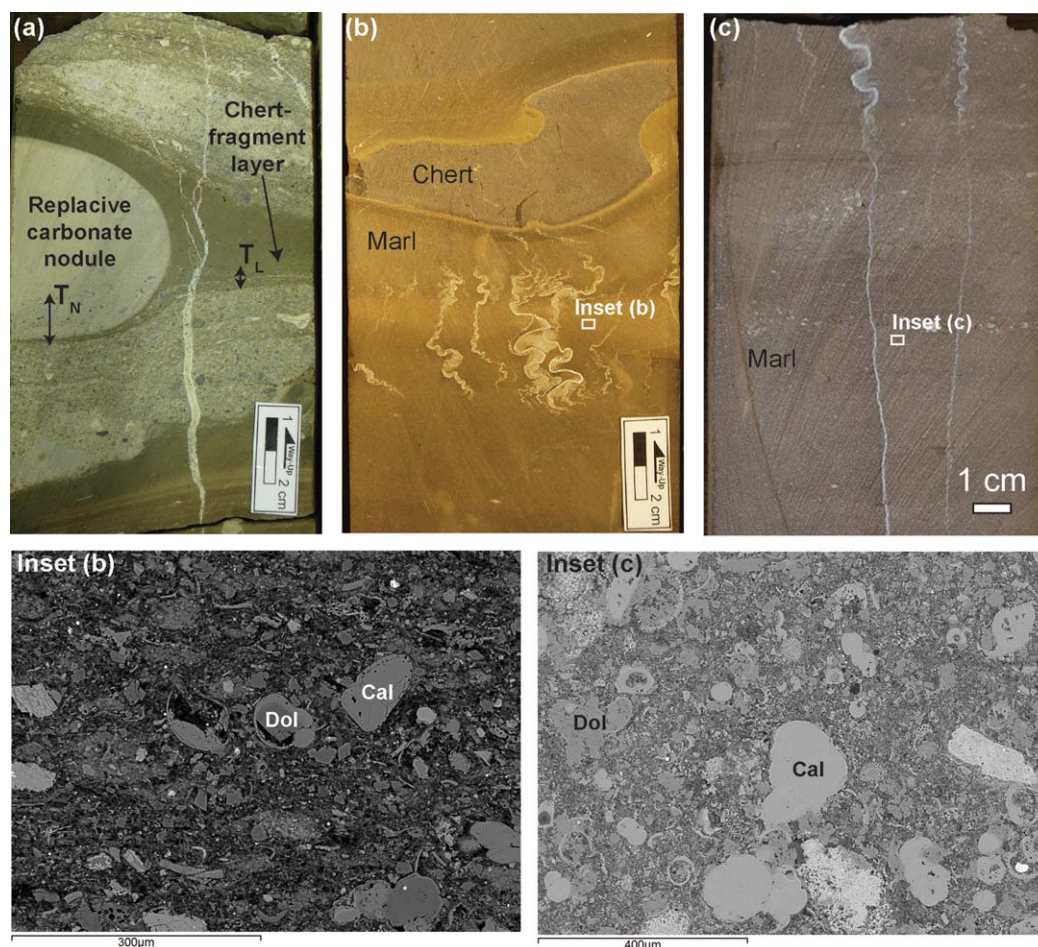


Figure 11. Variable compaction around nodules and cemented layers in core. Cal, calcite; Dol, dolomite. (a) Compaction precluded within carbonate nodule, Core 3 Unit A, producing greater thickness of laminae within the nodule (T_N) than outside (T_L). (b) Layer of compacted veins, Core 2 Unit A. Note gray chert nodule upsection. (inset) (b) BSE image from compacted vein layer in Figure 11b. Mouldic pores are partially or fully cemented; cement often has euhedral forms, such as the labeled dolomite rhomb. Abundant pore space remains in the matrix. Many microfossils are crushed. These observations suggest that cementation proceeded slowly amid compaction, and that minor cementation did little to prevent the collapse of the sedimentary framework, with accompanying folding of veins. (c) Marl interval with straight calcite veins, Core 2 Unit A. Note compacted veins upsection possibly represent continuations of the same straight veins. (inset) (c) BSE image from straight-vein layer in Figure 11c. Relative to the cement in Figure 11b, cement in Figure 11c fully fills microfossils and pervasively cements the microporous structure of the matrix. Microfossils in Figure 11c are generally intact. These observations suggest that cementation in the straight-vein layer in Figure 11c precluded compaction, in the same way that nodule cement precludes compaction elsewhere (Figure 6a).

Unit C suggests that the fractures either followed silicification, or vice versa, or the two processes were intertwined. If fracturing enabled or facilitated silicification by delivery of silica-saturated fluids, then we would expect those fractures to be dominantly filled by silica cements. Some chert-hosted fractures are silica cemented, but 76% of fractures logged within cherts are filled by calcite (Table 1). Rather, we interpret that the silicified intervals were relatively fracture prone, presumably via increased stiffness, at the time the fractures formed. In that case, the fracture arrangement is consistent with fracturing driven by uniform remote extension, with fractures preferentially developed in the stiffer, silicified layers, in which the resulting tensile stresses were highest.

This interpretation is also consistent with through going faults splaying into planar veins within chert layers (Figures 3a and 3c). As shown by *Ferrill et al.* [2014], uniform applied stresses may lead to shear failure in incompetent layers and hybrid failure or jointing in intervening stiff layers. Thus, the opening-mode fractures within cherts likely formed to accommodate the offset of the faults cutting the marl layers. Alternatively, slip upon the faults may have introduced fluids that elevated fluid pressure and so led to opening-mode fracture of chert beds, but it is unclear why such fractures did not also form within marls.

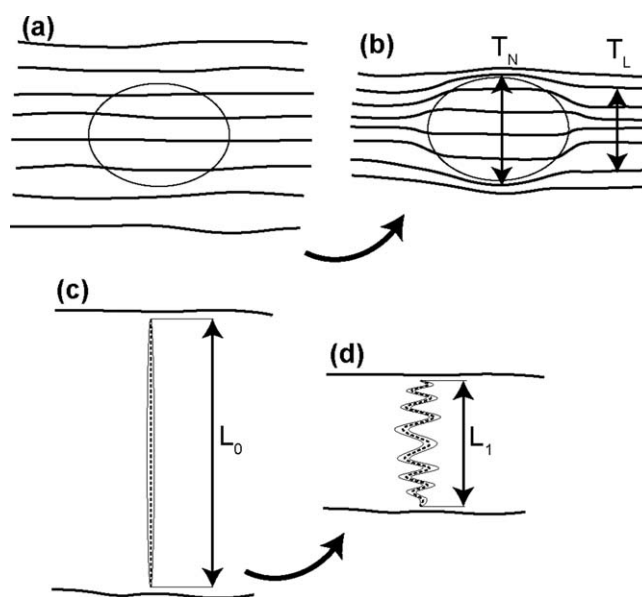


Figure 12. Illustration of compaction quantification around nodules and folded veins. T_N , thickness between the layers immediately above and below the nodule (uncompacted bedding thickness); T_L , thickness between same horizons, lateral to the nodule (compacted bed thickness); L_0 , meandering length of folded veins (uncompacted vein height); L_1 , straight-line distance between tips of folded veins (compacted vein height). (a) Nodule before compaction. (b) Nodule after compaction. (c) Vein before compaction. (d) Vein after compaction. Compaction ratio is (T_N/T_L) or (L_0/L_1) .

folded calcite veins also formed amid significant compaction. If opal CT is a precursor mineral to chert, then the silicification of nodules may have produced an intermediate gel-like phase consisting of unconsolidated opal CT lepispheres [Knauth, 1994]. As such, the onset of silicification may predate the extent of compaction plotted in Figure 13. As well, diffuse cements could prevent the host material around nodules from compacting (Figure 11c), in which case again the nodules may be older than implied by the amount of compaction around them.

In addition, our line-length calculation for compaction around folded veins (equation (2)) is probably a conservative estimate of the total compaction since the veins formed, for two reasons. First, the linear relationship between fracture width and fold-wavelength (Figure 7d) is consistent with buckle folding theory, in which the matrix undergoes some shortening before folding of the stiff layer begins [Cobbald, 1975]. Second, because the folding appears to be enabled by a combination of pressure solution within the calcite vein (Figure 7c) and calcite precipitation within microfractures within the inner arcs of folds (Figures 7a and 7b), we might anticipate that the folds will become “locked up,” as discussed for example by Ramsay [1974] for chevron folds. Further shortening of the matrix, beyond what is measured from the folds, is evident from wrapping of sediments around folded veins (Figures 6a and 8b). As such, our

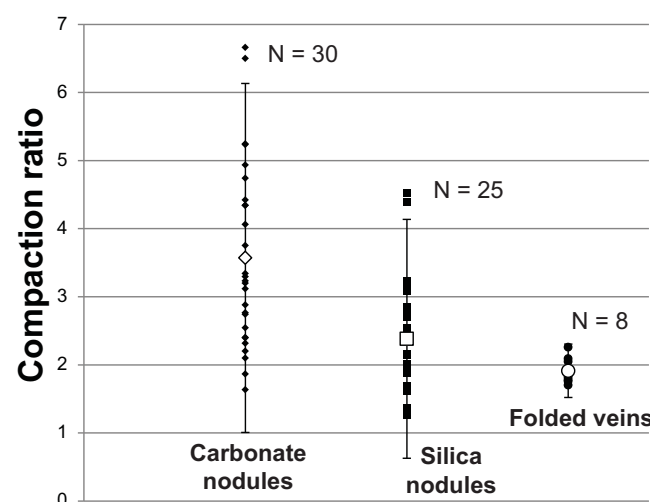


Figure 13. Compaction ratios measured for carbonate nodules, silica nodules, and folded veins. Black symbols are individual measurements; white symbols are averages; error bars represent two standard deviations.

In Unit A, the folded fractures are closely spaced in horizons in between chert beds. The horizons that contain folded fractures were likely not more brittle than the unfractured layers, given their high compactibility. Alternative mechanisms to remote extension, such as local fluid overpressures or volume changes associated with silicate phase transitions, might better explain the distribution of folded fractures.

6.2. Burial Diagenesis and Fracturing

Here we synthesize the results from compaction analyses, mineral assemblages and their overlapping relations, fluid inclusion observations, and cross-cutting relationships to infer the structural-paragenetic sequence within the cored section (Figure 14).

Calcite precipitation initiated very early in the burial history, based on the compaction ratios around replacive carbonate nodules. Silica nodules and

folded calcite veins also formed amid significant compaction. If opal CT is a precursor mineral to chert, then the silicification of nodules may have produced an intermediate gel-like phase consisting of unconsolidated opal CT lepispheres [Knauth, 1994]. As such, the onset of silicification may predate the extent of compaction plotted in Figure 13. As well, diffuse cements could prevent the host material around nodules from compacting (Figure 11c), in which case again the nodules may be older than implied by the amount of compaction around them.

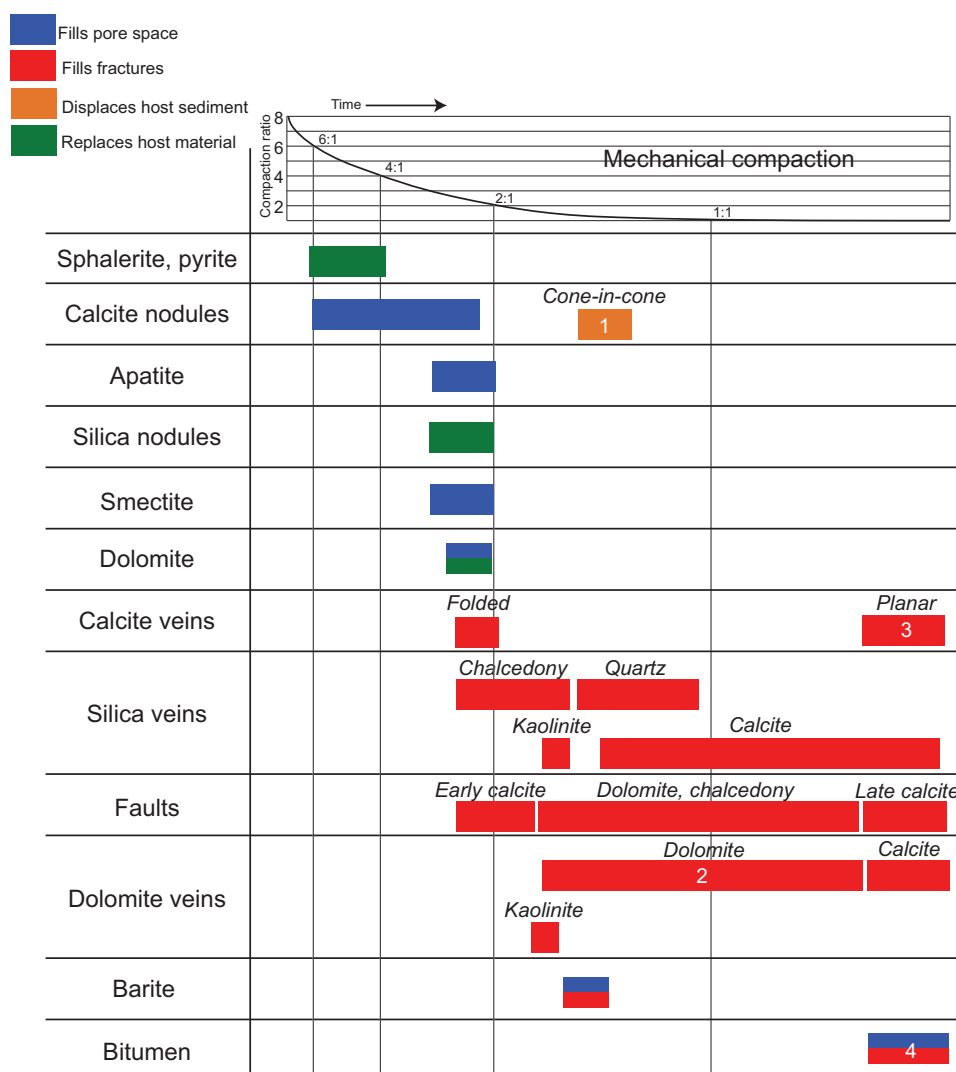


Figure 14. Paragenetic sequence of Jordan host-rock and fracture cements. Timing of sphalerite, pyrite, apatite, smectite from Huggett *et al.* [2017]. Notes: (1) cone-in-cone likely forms syn-lithification, postearliest host-sediment dolomite. (2) Fracture dolomite postdates host-sediment dolomitization. (3) Planar calcite veins paired with late calcite in faults based on isotopic grouping. (4) Bitumen paired with late calcite based on onlapping cement.

compaction calculations represent minimum estimates of the true compaction since both silicification of nodules and calcite veining.

On the basis of their similar compaction ratios, and considering that both measurement types are probably conservative estimates of the true compaction since formation, we interpret the chert nodules and compacted calcite veins to have formed coevally.

Faults include distributed strain consistent with plastic sediment deformation. This deformation is typically crosscut by brittle fractures, including discrete fault planes (Figures 3c and 3d). Fault zones also include each major cement phase we identified in the opening-mode fracture sets (Figures 3a–3d). We therefore conclude that faulting began prelithification and proceeded throughout opening-mode fracturing and diagenesis.

Dolomite veins likely initiated after the beginning of calcite precipitation but before compaction ceased, based on minor folding at nodule boundaries (Figure 5a) and the presence of kaolinite cement. Kaolinite was interpreted as early based on association with silica cements in fractures and diatoms being the likely source of aluminum in the absence of feldspar and clay [Huggett *et al.*, 2017]. Dolomite veins also contain

chalcedony, which appears intergrown with dolomite, suggesting coprecipitation. We infer a timing of chalcedony-bearing and dolomite-bearing fractures toward the final stages of mechanical compaction. Dolomite and microquartz fracture cements bear single-phase aqueous fluid inclusions, consistent with a low temperature of precipitation. These cements are present within layer-parallel fractures, implying fluid overpressure during formation, because the overburden should have supplied a compressive force against fracture opening. The internal pressure could theoretically be supplied by crystallization pressure, but the botryoidal chalcedony and euhedral dolomite belie this interpretation in favor of crystals growing into an overpressured fluid.

Calcite in veins formed at several different stages. We have described folded calcite veins which appear to have undergone significant compaction, during and after opening, consistent with an early timing of formation. We also note that calcite overlaps kaolinite, dolomite, and silica cements in veins (Figure 5b) and faults (Figure 3d). Planar calcite veins appear to postdate compaction and have sparser and thinner twins than those of their folded counterparts (Figure 4c). Therefore, development of calcite veins persisted throughout the burial and uplift history of the rocks, although likely from different sources and in fractures that opened in response to different mechanisms.

Planar calcite veins may have formed from tectonic stretching after thorough compaction and precipitation of the early diagenetic phases. However, in some cases compaction appears to have been halted by pore-filling cements that are not recognizable in core as nodules (Figure 11c). As mentioned above, the presence of these pore-filling cements suggest that some planar calcite veins may have the same timing as the folded calcite veins; such planar veins were not folded because their host beds were cemented early and prevented from compacting. However, in most cases we observed, the host-rock around planar calcite veins does not have pore space for significant cement to have been precipitated. Consistent with increased twin thickness and density within folded calcite veins, this suggests a later timing to planar calcite veins.

Planar calcite veins in marls are also more commonly present in parallel sets (Figure 4d) than are the poorly aligned folded veins (Figure 6b) and planar veins within nodules (Figure 5c). This alignment might reflect propagation under greater differential horizontal stress, which might be expected during deeper burial and amid a more tectonically imposed stress field than that of the early folded and nodular fractures.

Opal A forms at low temperature and is here likely produced by microorganisms. Opal A is undersaturated and will tend to dissolve in the water column, but if buried, dissolution can result in supersaturation with respect to opal CT, chalcedony, and quartz [Williams and Crerar, 1985]. Many silica veins in Jordan follow a commonly observed diagenetic sequence in which pores (fractures) are lined by chalcedony, which is overlapped by progressively coarsening quartz crystals. Although consistent with increasing temperature of precipitation, this sequence is more simply explained by an Ostwald ripening process, whereby tiny crystals of a highly soluble mineral (here, opal A) dissolve and reprecipitate to form coarser crystals of the same mineral, which then later dissolve to form crystals of a less soluble mineral, again with progressively coarsening grain size [Williams and Crerar, 1985].

Whatever the details of the silica transformation process, we infer that silica-filled fractures opened during the series of dissolution-precipitation reactions that transforms opal A into quartz. This interpretation is largely based on fracture-porosity-filling chalcedony and microquartz cements, consistent with both increasing temperature and Ostwald ripening of silica species. Because hydrous opal CT and chalcedony remain in the rocks, we infer that these phases were metastably present in a P–T field in which quartz precipitated from solution. The fractures do not appear to have contained opal, and many also contain dolomite coprecipitated with chalcedony according to which mineral formed the substrate.

Fracturing during steadily increasing temperature is consistent with fracturing beginning during compaction and proceeding through prograde burial, with coincident tectonism. The latest structures (planar calcite veins, faults) may have formed in response to tectonic stretching under temperatures up to the maximum experienced by these rocks. Indeed, regional fault patterns and the amount of displacement along cored faults are both consistent with significant tectonic deformation of the rocks.

6.3. Silica Diagenesis as Fracture Mechanism for Folded Calcite Veins

It has long been appreciated that diagenetic reactions can cause fracturing of sediments and rocks. Such fracturing has been interpreted to result from swelling, because the products have a greater volume than the reactants, and force the host material to fracture in order to make room [see Okamoto and Shimizu, 2015, for modeling and discussion]. Volume swelling reactions previously argued to produce fracturing

include anhydrite hydration [Shearman *et al.*, 1972], dolomitization [Bellamy, 1977], granulite-facies partial melting [Watt *et al.*, 2000], and peridotite carbonation [Kelemen and Matter, 2008].

Volume-reducing reactions can also cause fracturing. For example, coal commonly develops pervasive fracture networks, which are likely at least partially triggered by volume loss during maturation [Laubach *et al.*, 1998]. Volume loss during silica diagenesis has been argued to produce silica-filled fractures [Eichhubl and Boles, 1998; Maher and Shuster, 2012]. However, in contrast to fractures generated by swelling chemical reactions, for fractures that form via volume reductions it is not immediately clear what should fill the fractures. We argue below that volume loss related to silica diagenesis forced open the folded calcite veins.

The stratigraphic distribution, inferred timing, and volumetric strain manifest in the folded veins are all consistent with silica diagenesis as the primary driver of fracturing. We interpret the chert to originate from the transformation of biogenic opal A into opal CT, chalcedony, and quartz [Knauth, 1994]. This interpretation is consistent with the stratified, regionally correlable extent of the chert and with the presence of radiolaria. Folded veins are systematically located within marl layers adjacent to chert nodules—including examples that cut chert layers and are folded above and below (Figure 6a). Overlapping compaction ratios (Figure 13) suggest that the folded veins formed at the same time as the chert nodules. Thus, the folded veins and silica nodules coincide in space and are inferred to have coincided in time.

We can estimate the volumetric fraction of any host-rock layer comprising folded veins. We take the cross section observed in core face to be representative of a volume of rock having an arbitrarily large third dimension parallel to fracture strike, and we assume plane fracture-strain. The cross-sectional area of each vein, precompaction, can be approximated as an ellipse, with the minor axis being the fracture aperture and the major axis the layer height, considering that most folded veins are height restricted. The cross-sectional area of the host layer is the core width—generally 10 cm—times the layer height. The fractured volume is then the ratio between the summed-fracture and host-rock areas:

$$\frac{\frac{1}{4}\pi a \sum b}{aw} \quad (3)$$

where a is the layer thickness and height of the fractures, w is the core width, and $\sum b$ is the sum of all fracture apertures in the layer. Equation (3) simplifies to

$$\frac{\pi \sum b}{4w} \quad (4)$$

Taking the average summed aperture for folded veins at any given core depth = 2.06 mm (Table 2), we calculate an average fracture volume of 1.62%; the summed-fracture aperture at two standard deviations above the average is 4.78 mm, corresponding to a fracture volume of 3.75%.

To conservatively estimate of the volume loss undergone by the marl layers as a result of silica diagenesis, we can calculate a volume of opal that would correspond to the observed volume of quartz currently in the host. Calculated density values [Deer *et al.*, 1992] are 2.65 g/cm³ for quartz and 2.33 g/cm³ for cristobalite. Calculating the bulk volume change as

$$\frac{(V_c - V_q)}{V_c} \quad (5)$$

where V_c is a given volume of pure cristobalite and V_q the equivalent transformed volume of quartz, conserving mass, the solid transformation of cristobalite to quartz would produce a 12% bulk volume loss.

Petrographic examination of the amount and composition of matrix within the Unit A marls (Figures 8 and 10) shows that siliceous mud content is consistently above 10% by volume, consistent with XRD measurements by Huggett *et al.*

Table 2. Fracture Cumulative Aperture Values, i.e., the Sum of All Vertical-Fracture Apertures Within Each Layer^a

	Nonnodular		Nodular (Planar)	
	Folded	Planar	Carbonate	Silica
Average	2.06	1.37	1.11	1.71
Standard deviation	1.36	1.60	0.85	2.15
Median	1.81	0.89	0.73	1.06

^a“Carbonate” and “silica” refer to the nodule mineralogy, not the vein fill. Compiled from log of Cores 1– and 5.

[2017]. Therefore, the corresponding volume loss would be at least 1.2% in the host sediment. However, the true volume loss is likely greater. Cristobalite is denser than tridymite and both are denser than natural opals, owing to opal's several weight-percent bound-water content [Graetsch, 1994]. Using 2.09 g/cm^3 as a typical density of opal [Deer *et al.*, 1992], the implied minimum bulk volume loss is 21%, or 2.1% of the Unit A marls.

The microporous structure of siliceous microorganisms implies still higher volumes of precursor silica. Although the siliceous mud appears to have been well mixed with the nonsiliceous components, as a lower extreme we can assume the siliceous mud had a density similar to natural diatomite, i.e., 0.3 g/cm^3 [Inglethorpe, 1993]. Using this value, the minimum bulk volume loss would be 89% for the siliceous mud and 8.9% for the composite marl.

Finally, petrographic evidence shows that the production of chert nodules incorporated silica from the marl layers. Remobilization of silica at the bed scale is evident in replaced, undamaged, originally carbonate tests within cherts (Figure 8e) and corresponding carbonate-cemented radiolaria within marls (Figure 8c). The chert grew by replacing both fluids and carbonate constituents in the original host material, and the neighboring marls are evidently depleted in silica. This depletion implies a greater original volume of biogenic opal, which was lost during silicification of chert nodules, than is accounted for in the above density calculations. Therefore, 2–4% volumetric fracturing is well within the potential limits achievable by silica diagenesis.

We consider it most likely that the fractures were driven open in response to silica diagenesis, as opposed to crustal stretching or fluid overpressures. Crustal stretching may preferentially fracture chert layers, if cherts are more brittle [e.g., Gross *et al.*, 1995] by virtue of their abundant quartz and lack of organic matter. Indeed, we observe that many chert beds are preferentially fractured, with planar calcite veins, relative to surrounding marls (Figure 4a). In contrast, folded fractures are clustered between chert beds, in layers that were unsilicified and therefore likely not more brittle than the unfractured layers, especially at this early stage of compaction. Therefore, the folded fractures are difficult to attribute to crustal stretching.

6.4. Role of Fluids

Fluid overpressures can develop within compacting, dewatering sediments, and potentially drive fractures open [Cosgrove, 1995]. The development of such overpressures may have been assisted by early cementation of pore spaces, which would have reduced the already low permeability of the fine-grained host sediment. However, such cement would also have precluded the folding of the veins. If overpressures caused by chert formation preventing dewatering were the primary driver of fracture opening, then we might expect to see folded veins preferentially developed beneath the chert beds. Instead, we observe that the fractures are just as common above chert beds (Figure 6c). Furthermore, it is likely that the nodular geometry of many chert bodies has too narrow a lateral extent to have prevented fluid escape during compaction.

Nevertheless, fluid overpressures may certainly have assisted in the formation of the folded veins, as it likely did for layer-parallel veins, as discussed above. High fluid pressure can help to explain why opening-mode fractures formed rather than faults [Cosgrove, 1995], which have previously been attributed to silica diagenesis [Cartwright, 2011]. The diagenetic fracture mechanism discussed above focuses on the solid-fraction volume change, but of course silica diagenesis involves the expulsion of water, whether by syneresis [Rapson, 1962] or simple dissolution of hydrous microfossils. This fluid expulsion could have created local fluid overpressures, although these would likely have been ephemeral in the unconsolidated sediment.

The immaturity of the considerable organic material in the sediment precludes significant overpressure due to catagenesis. However, fracturing has been attributed to early-burial overpressure related to methanogenic bacteria [Meng *et al.*, 2017], which feed on organic material in the shallow subsurface. We also speculate that the high organic content in the sediment could have reduced the effective aqueous permeability, and so magnified any overpressures which might have otherwise been efficiently bled away.

6.5. Simultaneous Silica and Carbonate Diagenesis

That the folded veins filled with calcite as they opened suggests that the pore water was supersaturated with respect to calcite throughout compaction and silica diagenesis. The space previously occupied by silica in the unsilicified layers is now at least partially occupied by carbonate cement, as shown by the calcitized radiolaria (Figure 8c). Petrographically indistinguishable carbonate cement filled fractures as they opened and were folded. In principle, rapid carbonate precipitation could have prevented diagenetic fracturing by

filling the space vacated by mobilized silica, thus preventing the contraction of the host-rock. It is likely, however, that the microporous matrix inhibited calcite nucleation except in relatively large pores such as dissolved radiolaria and fractures. Therefore, calcite did not replace missing silica molecule-by-molecule during opal dissolution, and hence did not prevent contraction of the matrix.

Classically, the simultaneous precipitation of carbonate and silicate minerals has been viewed as problematic, such that apparent co-precipitation of these minerals has been attributed to high magnitude and frequency changes in pH [e.g., Rapson, 1962]. The apparent problem comes from assuming that geologic fluids are at their equilibrium saturation, and that the presence of a mineral precipitation implies some process that moved the fluid toward supersaturation [e.g., Gratier *et al.*, 2012]. It has since been appreciated that mineral precipitation is commonly limited by kinetics [e.g., Walderhaug, 1996], meaning that fluids are supersaturated with minerals, and so pH, pressure, temperature, and even dissolved mineral supply may vary considerably over time without interrupting crystal growth. Accordingly, it has been shown that quartz and calcite can truly co-precipitate, at least at low-grade metamorphic conditions [Kirschner *et al.*, 1995]. In the present case, supersaturation with respect to quartz was likely driven by dissolution of biogenic opal, and so the presence of quartz poses no problem for the continued precipitation of calcite. This interpretation is consistent with coeval fracture opening and chert nodule formation, along with crack-seal texture indicating simultaneous calcite precipitation into fractures during fracture opening.

6.6. General Significance

The presence of early, compacted fractures in a formation formed largely of originally amorphous silica was also noted by Ramseyer *et al.* [2013]. Although the silica was attributed to inorganic precipitation from seawater rather than siliceous organisms, the volume changes undergone by the silica in that study could also have generated fractures. By extension, diagenetic triggers should be considered for other documented examples of compacted fractures [Hiscott, 1979; Gasparrini *et al.*, 2013].

More broadly, we suggest that, because the failure of rock reflects the summation of all applied stresses, to correctly interpret the dynamics between subsurface fracturing and fluid flow requires consideration of all the sources of stress. Therefore, even where tectonic structures dominate the geology, it should be remembered that fractures reflect not just crustal deformation but also thermal [English, 2012], catagenetic [Hooker *et al.*, 2017], and, of course, diagenetic stresses.

7. Conclusions

The Cretaceous-Paleogene of Jordan contains a highly stratified fracture pattern. The original host strata guided the development of natural fractures throughout compaction and tectonism via several diagenetic processes. Most important among these processes was silica diagenesis, which not only embrittled certain layers, but likely drove the host-rocks to failure, resulting in the development of now-folded calcite veins. Carbonate diagenesis was simultaneously active, as evident from crack-seal texture within folded calcite veins, and dolomitization of host-rocks and fracture pore space.

The folded veins highlight the potential for uncompacted sediments to form calcite veins during, and likely in response to, silica diagenesis. Therefore, the hydraulic and mechanical properties of a variety mudrocks may be dominated by fractures, even very early in their burial history and in the absence of tectonic deformation. Moreover, silica diagenesis creates fractures via contraction of the host material, and these fractures may be filled with material unrelated to the reaction that formed them.

Acknowledgments

This work has been funded by Shell International Exploration and Production B.V. We are grateful to M. Alqudah, I. Abu-Mahfouz, S. van den Boorn, O. Podlaha, M. Gross, R. Pierpont, and P. Van Rensbergen for helpful discussion, and to Editor C.-T. Lee and two anonymous reviewers. Please contact J.N.H., john.hooker@earth.ox.ac.uk, for data used in this study.

References

- Abu-Jaber, N. S., M. M. Kimberley, and V. V. Cavaroc (1989), Mesozoic-Paleogene basin development within the eastern Mediterranean borderland, *J. Pet. Geol.*, 12(4), 419–436.
- Ali Hussein, M., M. Alqudah, G. Podlaha, O. G., van den Boorn, S., Kolonic, and J. Mutterlose (2014), Ichnofabrics of Eocene oil shales from central Jordan and their use for paleoenvironmental reconstructions, *GeoArabia*, 19(1), 145–160.
- Alqudah, M., M. Ali Hussein, O. G. Podlaha, S. van den Boorn, S. Kolonic, and J. Mutterlose (2014), Calcareous nannofossil biostratigraphy of Eocene oil shales from central Jordan, *GeoArabia*, 19(1), 117–140.
- Bellamy, J. (1977), Subsurface expansion megapolygons un Upper Jurassic dolostone (Kimmeridge, UK), *J. Sediment. Petrol.*, 47, 973–978.
- Bourne, S. J. (2003), Contrast of elastic properties between rock layers as a mechanism for the initiation and orientation of tensile failure under uniform remote compression, *J. Geophys. Res.*, 108(B8), 2395, doi:10.1029/2001JB001725.

- Cartwright, J. (2011), Diagenetically induced shear failure of fine-grained sediments and the development of polygonal fault systems, *Mar. Pet. Geol.*, **28**, 1593–1610.
- Cobbold, P. R. (1975), Fold propagation in single embedded layers, *Tectonophysics*, **27**, 333–351.
- Cooke, M. L., and C. A. Underwood (2001), Fracture termination and step-over at bedding interfaces due to frictional slip and interface opening, *J. Struct. Geol.*, **23**, 223–238.
- Cosgrove, J. W. (1995), The expression of hydraulic fracturing in rocks and sediments, in *Fractography: Fracture Topography as a tool in Fracture Mechanics and Stress Analysis*, edited by M. S. Ameen, *Geol. Soc. London Spec. Publ.*, **92**, 187–196.
- Deer, W. A., R. A. Howie, and J. Zussman (1992), *An Introduction to the Rock-Forming Minerals*, 2nd ed., 696 pp., John Wiley, New York.
- Eichhubl, P., and J. R. Boles (1998), Vein formation in relation to burial diagenesis in the Miocene Monterey Formation, Arroyo Burro beach, Santa Barbara, California, in *Diagenesis, Deformation, and Fluid Flow in the Miocene Monterey Formation*, edited by P. Eichhubl, *Pac. Sect. SEPM Spec. Publ.*, **Book 83**, 15–36 plus figs.
- English, J. M. (2012), Thermomechanical origin of regional fracture systems, *AAPG Bull.*, **96**(9), 1597–1625.
- Ferrill, D. A., R. N. McGinnis, A. P. Morris, K. J. Smart, Z. T. Sickmann, M. Bentz, D. Lehrmann, and M. A. Evans (2014), Control of mechanical stratigraphy on bed-restricted jointing and normal faulting: Eagle Ford Formation, south-central Texas, *AAPG Bull.*, **98**(11), 2477–2506.
- Gasparrini, M., W. Sassi, and J. F. W. Gale (2013), Natural sealed fractures in mudrocks: A case study tied to burial history from the Barnett Shale, Fort Worth Basin, Texas, USA, *Mar. Pet. Geol.*, **55**, 122–141.
- Giorgioni, M., A. Iannace, M. D'Amore, F. Dati, L. Gallucio, V. Guerriero, S. Mazzoli, M. Parente, C. Strauss, and S. Vitale (2016), Impact of early dolomitization on multi-scale petrophysical heterogeneities and fracture intensity of low-porosity platform carbonates (Albian–Cenomanian, southern Apennines, Italy), *Mar. Pet. Geol.*, **73**, 462–478.
- Graetsch, H. (1994), Structural characteristics of opaline and microcrystalline silica minerals, in *Silica: Physical Behavior, Geochemistry, and Materials Application*, edited by P. T. Heaney, C. T. Prewitt, and G. V. Gibbs, *Rev. Mineral. Geochem.*, **29**, 207–232.
- Gratier, J.-P., E. Frery, P. Deschamps, A. Røyne, F. Renard, D. Dysthe, N. Ellou-Zimmerman, and B. Hamelin (2012), How travertine veins grow from top to bottom and lift the rocks above them: The effect of crystallization force, *Geology*, **40**(11), 1015–1018.
- Gross, M. R., M. P. Fischer, T. Engelder, and R. J. Greenfield (1995), Factors controlling joint spacing in interbedded sedimentary rocks: Integrating numerical models with field observations from the Monterey Formation, USA, in *Fractography: Fracture Topography as a Tool in Fracture Mechanics and Stress Analysis*, edited by M. S. Ameen, *Geol. Soc. London Spec. Publ.*, **92**, 215–233.
- Gudmundsson, A., and S. L. Brenner (2001), How hydrofractures become arrested, *Terra Nova*, **13**(6), 456–462.
- Hiscott, R. N. (1979), Clastic sills and dikes associated with deep-water sandstones, Tourelle Formation, Ordovician, Quebec, *J. Sediment. Petrol.*, **49**(1), 1–10.
- Hooker, J. N., and J. Cartwright (2016), Dolomite inclusions suggest a primary origin of cone-in-cone, *Geol. Mag.*, doi:10.1017/S0016756816000807, in press.
- Hooker, J. N., S. E. Laubach, and R. Marrett (2013), Fracture-aperture size—Frequency, spatial distribution, and growth processes in strata-bounded and non-strata-bounded fractures, Cambrian Mesón Group, NW Argentina, *J. Struct. Geol.*, **54**, 54–71.
- Hooker, J. N., S. E. Laubach, and R. Marrett (2014), A universal power-law scaling exponent for fracture apertures in sandstones, *GSA Bull.*, **126**(10), 1340–1362.
- Hooker, J. N., J. Cartwright, B. Stephenson, C. Silver, A. J. Dickson, and Y.-T. Hsieh (2017), Fluid evolution in fracturing black shales, Appalachian Basin, *AAPG Bull.*, doi:10.1306/10031616030, in press.
- Huggett, J., J. N. Hooker, and J. Cartwright (2017), Lithologic controls on diagenesis and diagenetic sequence in the Al Hasa phosphorite, Muwaqqar chalk marl, and Um Rijam chert formations, Jordan, *Arabian J. Geosci.*, **10**, 270, doi:10.1007/s12517-017-3038-5.
- Inglethorpe, S. D. J. (1993), Industrial minerals laboratory manual: Diatomite, *Br. Geol. Surv. Tech. Rep. WG/92/39*, 37 pp., Nat. Environ. Res. Council, Keyworth, U. K.
- Jochum, J., G. Friedrich, D. Leythaeuser, R. Littke, and B. Ropertz (1995), Hydrocarbon-bearing fluid inclusions in calcite-filled horizontal fractures from mature Posidonia Shale (Hils Syncline, NW Germany), *Ore Geol. Rev.*, **9**, 363–370.
- Kelemen, P. B., and J. Matter (2008), In situ carbonation of peridotite for CO₂ storage, *Proc. Natl. Acad. Sci., U. S. A.*, **105**(45), 17,295–17,300.
- Kirschner, D. L., Z. D. Sharp, and H. Masson (1995), Oxygen isotope thermometry of quartz-calcite veins: Unraveling the thermal-tectonic history of the subgreenschist facies Morcles nappe (Swiss Alps), *GSA Bull.*, **107**(10), 1145–1156.
- Knauth, L. P. (1994), Petrogenesis of chert, in *Silica: Physical Behavior, Geochemistry, and Materials Application*, edited by P. T. Heaney, C. T. Prewitt, and G. V. Gibbs, *Rev. Mineral. Geochem.*, **29**, 233–258.
- Laubach, S. E., R. Marrett, J. E. Olson, and A. R. Scott (1998), Characteristics and origins of coal cleat: A review, *Int. J. Coal Geol.*, **35**, 175–207.
- Laubach, S. E., J. E. Olson, and M. R. Gross (2009), Mechanical and fracture stratigraphy, *AAPG Bull.*, **93**(11), 1413–1426.
- Lavenue, A. P. C., J. Lamarche, A. Gallois, and B. D. M. Gauthier (2013), Tectonic versus diagenetic origin of fractures in a naturally fractured carbonate reservoir analog (Nerthe anticline, southeastern France), *AAPG Bull.*, **97**(12), 2207–2232.
- Lüning, S., and J. Kuss (2014), Petroleum geology of Jordan, in *Petroleum Systems of the Tethyan Region*, edited by L. Marlow, C. Kendall, and L. Yose, *AAPG Mem.*, **106**, 217–239.
- Maher, H., Jr., and R. Shuster (2012), Chalcedony vein horizons and clastic dikes in the White River Group as products of diagenetically driven deformation, *Lithosphere*, **4**(3), 167–186.
- Meng, Q., J. N. Hooker, and J. Cartwright (2017), Early overpressuring in organic-rich shales during burial: Evidence from fibrous calcite veins in the Lower Jurassic Shales-with-Beef Member in the Wessex Basin, UK, *J. Geol. Soc.*, doi:10.1144/jgs2016-146, in press.
- Okamoto, A., and H. Shimizu (2015), Contrasting fracture patterns induced by volume-increasing and -decreasing reactions: Implications for the progress of metamorphic reactions, *Earth Planet. Sci. Lett.*, **417**, 9–18.
- Ortega, O. J., J. F. W. Gale, and R. Marrett (2010), Quantifying diagenetic and stratigraphic controls on fracture intensity in platform carbonates: An example from the Sierra Madre Oriental, northeast Mexico, *J. Struct. Geol.*, **32**, 1943–1959.
- Powell, J. H., and B. K. Moh'd (2011), Evolution of Cretaceous to Eocene alluvial and carbonate platform sequences in central and south Jordan, *GeoArabia*, **16**(4), 29–82.
- Price, N. J. (1966), *Fault and Joint Development in Brittle and Semi-Brittle Rock*, 176 pp., Pergamon, Oxford, U. K.
- Ramsay, J. G. (1974), Development of chevron folds, *GSA Bull.*, **85**, 1741–1754.
- Ramsay, J. G. (1980), The crack-seal mechanism of rock deformation, *Nature*, **284**, 135–139.
- Ramseyer, K., J. E. Amthor, A. Matter, T. Pettke, M. Wille, and A. E. Fallick (2013), Primary silica precipitate at the Precambrian/Cambrian boundary in the South Oman Salt Basin, Sultanate of Oman, *Mar. Pet. Geol.*, **39**, 187–197.
- Rapson, J. E. (1962), The petrography of Pennsylvanian chert breccias and conglomerates: Rocky Mountain Group, Banff, Alberta, *J. Sediment. Petrol.*, **32**(2), 249–262.
- Sellés-Martínez, J. (1996), Concretion morphology, classification and genesis, *Earth Sci. Rev.*, **41**, 177–210.

- Shackleton, J. R., M. L. Cooke, and A. J. Sussman (2005), Evidence for temporally changing mechanical stratigraphy and effects on joint-network architecture, *Geology*, *33*, 101–104.
- Shearman, D. J., G. Mossop, H. Dunsmore, and M. Martin (1972), Origin of gypsum veins by hydraulic fracture, *Trans. Inst. Min. Metall., Sect. B*, *81*, B149–B155.
- Ulven, O. I., H. Storheim, H. Austrheim, and A. Møller-Jensen (2014), Fracture initiation during volume increasing reactions in rocks and applications for CO₂ sequestration, *Earth Planet. Sci. Lett.*, *389*, 132–142.
- Walderhaug, O. (1996), Kinetic modeling of quartz cementation and porosity loss in deeply buried sandstone reservoirs, *AAPG Bull.*, *80*(5), 731–745.
- Watt, G. R., N. H. S. Oliver, and B. J. Griffin (2000), Evidence for reaction-induced microfracturing in granulite facies migmatites, *Geology*, *28*(4), 327–330.
- Williams, L. A., and D. A. Crerar (1985), Silica diagenesis, II. General mechanisms, *J. Sediment. Petrol.*, *55*(3), 312–321.
- Zhang, J., Z. Jiang, X. Jiang, S. Wang, C. Liang, and M. Wu (2016), Oil generation induces sparry calcite formation in lacustrine mudrock, Eocene of east China, *Mar. Pet. Geol.*, *71*, 344–359.